PROCEEDINGS, 51st Workshop on Geothermal Reservoir Engineering
Stanford University, Stanford, California, February 9-11, 2026
SGP-TR-230

# The Three Cs (Conductivity, Connectivity and Conformance) that Control the Performance of Enhanced Geothermal Systems: Lessons Learnt at the Forge EGS Site

Mukul M. Sharma and Yuhao Ou

University of Texas at Austin

msharma@mail.utexas.edu

**Keywords:** Enhanced Geothermal System, conductivity, conformance, connectivity

## ABSTRACT

The three most important factors controlling the performance of enhanced geothermal systems are, (i) the hydraulic conductivity of the fractures, (ii) the connectivity between the injection and production wells, and (iii) the fluid conformance in the injection well. Data obtained at the Forge EGS site and numerical simulations clearly show the importance of these three factors.

Good connectivity between the injector and the producer through fractures is essential to EGS success. This inter-well connectivity was measured with both fiber optic data in the producing well and through tracers. DSS (strain) measurements made in the producing well while the frac stages were being pumped in the injection well clearly showed the location and timing of the frac hits in the producing well. Over 48 different frac hits were recorded. To ensure good inter-well connectivity, the producing well was perforated at the location of the major frac-hits. To further improve inter-well connectivity hydraulic fractures were initiated through these perforation clusters in the producing well. Subsequent fluid circulation tests showed excellent connectivity between the injector and producer. Fluid inflow distribution along the producer was monitored by both DTS fiber measurements and tracer data. Both data sets were consistent and showed good inter-well connectivity.

Good fluid conformance is essential to avoid thief-fractures from causing early temperature breakthrough and a rapid decline in energy production rate over time. Large sections of the geothermal reservoir can remain undrained when this occurs. Fluid conformance in the producer was measured by DTS and by tracer tests. The results from the tracer test clearly show some preferred corridors of fractures indicating poor conformance in some parts of the wellbore. Ways to minimize this in the future are discussed. Simulations were run to show how this can be achieved in future EGS fracture designs.

Good fracture conductivity can be achieved by pumping proppant during the fracture treatment. In the first 3 stages of the fracture treatment of the 16A well at the Forge site, no proppant was pumped. This resulted in very large injection pressures being needed to inject fluid from the injector to the producer. All stages in which proppant was used were able to inject fluid at much lower pressures. The use of proppant results in better conductivity and is essential for maintaining injectivity and minimizing the parasitic energy needed to circulate fluid between the wells. Simulation results clearly show the impact of poor fracture conductivity and conformance on the energy recovery rate.

Ensuring good connectivity, conductivity and conformance in enhanced geothermal systems is shown to be critical for ensuring high and stable energy production rates.

## 1. INTRODUCTION

The optimum performance of Enhanced Geothermal Systems (EGS) can only be achieved if there is efficient heat transfer between the reservoir rock and the fluids circulated between the injector and producer through fractures. To achieve efficient heat transfer it is essential to (a) maximize the contact area between the rock and the injected fluid, (b) ensure that the injected fluid flows through all the fractures, and (c) minimize the pressure required to circulate the fluid so that parasitic power losses can be minimized. This paper addresses these central concerns through the learnings achieved at the Forge site and proposes ways in which this can be achieved.

## 2. BACKGROUND

### 2.1 An Overview of the Forge Site

Located near Milford, Utah, the FORGE site targets a hot dry rock granite formation at depths exceeding 3,000 meters and temperatures over 220°C, representing a milestone in the demonstration of full-scale EGS development (Figure 3.1a). It combines state-of-the-art horizontal drilling, multi-stage hydraulic stimulation, and fiber-optic distributed sensing to investigate fracture geometry, inter-well connectivity, and heat extraction efficiency in hot dry rock. As one of the first geothermal projects to apply distributed fiber sensing during both stimulation and circulation, FORGE has generated invaluable datasets that improve the understanding of subsurface heat and mass transfer in EGS.

The Utah FORGE test site features a geothermal circulation system consisting of a deviated injector well (16A) and a corresponding deviated producer well (16B) (Figure 1). Both wells, 16A and 16B, are long slanted wells with the producer 16B drilled above the injector, 16A. Aiming to establish connectivity with the production well 16B and increase the permeability of the geothermal reservoir between the wells, multi-stage hydraulic fracturing was applied to stimulate the injector 16A and increase the connectivity between injector and producer. Three stages of hydraulic fracturing stimulation were completed in April 2022 without proppant injection. Stages 3R to stage 10 in 16A were completed later in April 2024 with additional fracturing stages still to be planned. During most of these stages, proppant was used. Fracture diagnostic tools were employed to monitor the fracture intersections along the

production well 16B during the stimulation of 16A. 4 stages in 16B were then stimulated at detected intersections to establish good hydraulic connectivity between the two sets of fractures created in the injector and producer. Two major inter-well circulation tests were conducted: the first in July 2023 and the second in April 2024, conducted immediately after the April 2024 hydraulic fracturing campaign. During these tests, fluid was injected at fixed rates into well 16A and extracted from well 16B to test the connectivity of the created multi-fracture system.

To monitor the hydraulic stimulation and fluid circulation, a multi-mode fiber-optic cable was permanently cemented behind the casing of well 16B (Figure 2). This allowed for the deployment of distributed acoustic, temperature and strain sensing technologies (DAS, DTS and DSS data were all collected at the FORGE site) under extreme subsurface conditions. Notably, this system withstood prolonged exposure to high temperatures (> 220°C) and enabled distributed, real-time monitoring during both stimulation and EGS fluid circulation tests.

Circulation test 1

In the July 2023 fluid circulation test, fiber optic distributed strain sensing was used to monitor the possible fracture intersections along the production/monitoring well 16B and their responses during the EGS circulation. In the fiber optic strain rate waterfall that plots the strain rate with respect to measured depth along the producer and circulation time, tensional strain rate signals are seen in the zone of interest suggesting possible intersecting fractures and an overall expansion of the formation due to injection (Figure 3.3). Geometry characteristics of these observed tensional strain rate signals are expected to correlate with fracture conductivity and property changes in the stimulated reservoir volume (SRV).

April 2024 well stimulation

Hydraulic fractures in geothermal injection wells must intersect production wells so that good fluid communication can be maintained between the wells ensuring overall success in geothermal energy extraction (Jurick et al., 2025). In the FORGE April 2024 well stimulation of 16A and 16B, the deployed multi-mode fiber cable was employed to monitor fracture propagation with the aim of assessing the geometry and connectivity of the stimulated fracture network. Using the Rayleigh frequency shift based distributed strain sensing (DSS-RFS), the team continuously monitored fracture stimulation events originating from the adjacent injection well (stage 3R to stage 10 in 16A). These measurements enabled the detection of fracture-driven interactions, commonly referred to as “frac hits”, along the production well (Figure 3.4). The insights from the fiber optic data, interpreted as fracture intersections from the distributed strain data, were then used to guide the design and placement of perforation clusters in the production well (Figure 3.5). In the following production well stimulation (stage 1 to 4 in 16B), HF-DAS provided additional information regarding the fluid and proppant distribution during the fracturing injection (Figure 3.6). This data-informed strategy resulted in successful hydraulic fractures that effectively linked the injection and production wells, as later confirmed by cross-well circulation tests conducted after well stimulation (Ou et al., 2025).

Circulation test 2

Following the stimulation of production well 16B, fiber optic monitoring remained active throughout the April 2024 fluid circulation test. During the early stages of circulation, thermal slugging behavior, characterized by abrupt temperature changes along the wellbore, were observed in the fiber optic waterfall plot originating from the four perforated stages completed along well 16B (Figure 3.7). This phenomenon was attributed to heterogeneous thermal conditions within the wellbore, a residual effect of prior hydraulic stimulation. The gradient of these thermal slugs provided insight into fluid velocity variations along the producer 16B, illustrating the value of distributed fiber-optic sensing to resolve real-time subsurface flow dynamics with high sensitivity to localized thermal and hydraulic perturbations.

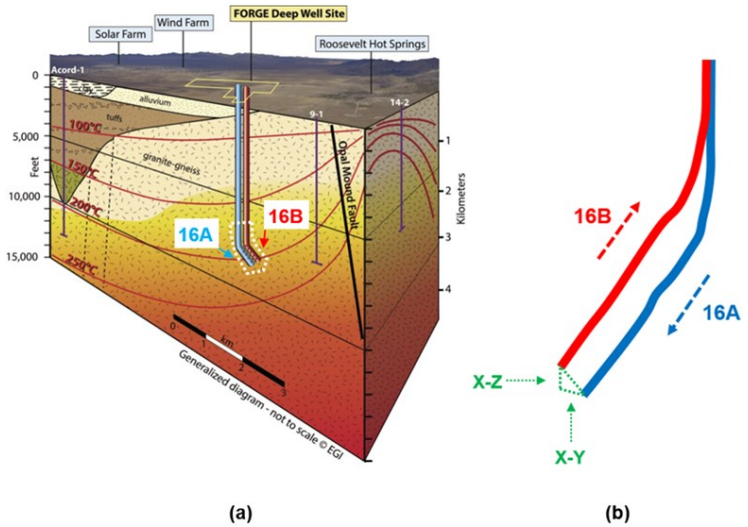


Figure 1: (a) General well placement of the Utah FORGE EGS test site. The EGS consists of one long deviated injector 16A (shown in blue color) and one deviated producer 16B placed above it (depicted in red color); (b) Well placement of the injection well 16A and production well 16B in the FORGE geothermal formation. The EGS well pair is 110 meters apart in the X-Z plane and a distance of 60 meters in the X-Y plane (Ou et al., 2025c).

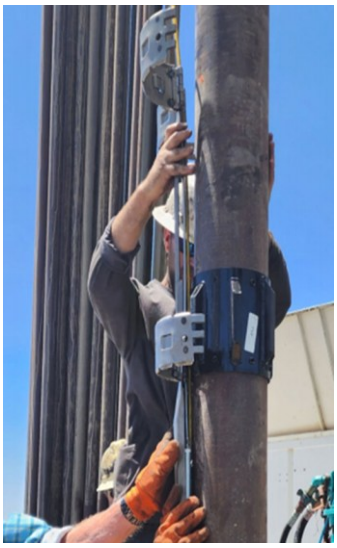

Figure 2: Fiber optic cable package (multi-mode and single mode) installed by the University of Texas-Shell team in the 16B well at the Utah-Forge site.

### 2.2 The Three Cs

As stated in the abstract, the primary factors governing the energy extraction rate in any EGS well pair are the three Cs:

- Conformance. Create uniformly placed fractures to ensure an even distribution of flow into all hydraulic fractures;
- Connectivity: Maximize the area of the created and connected fracture network through which the injected fluid flows;
- Conductivity: Create highly conductive fracture networks from the injector to the producer.

Innovations in integrated fracture diagnostics enabled us to monitor the performance of the injection-production well pair at Forge and conduct a detailed assessment of the effectiveness of different stimulation methods. This involved the use of fiber optic data as well as tracer data interpreted through numerical simulations. This design methodology can result in better connected and more uniform fractures and have a transformational impact on geothermal energy extraction by increasing the rate of energy extraction and reducing the energy extraction decline rate.

In the following sections of this paper, we discuss each of these critical factors; how they can be measured / monitored and how this can be used to improve EGS performance using the Forge site as an example.

## 3. FRACTURE CONDUCTIVITY

The first 3 fracture stages at Forge (Stages 1 to 3) were pumped in April 2022 without any proppant followed by additional stages (Stage 3R through Stage 10) in April 2024. The target formation beneath the FORGE site comprises hot, dry crystalline rock with a high density of natural fractures. This geological setting is conducive to the formation of complex hydraulic fracture networks, including small-scale branches and secondary fractures.

During July 2023 a fluid circulation test was conducted (for Stages 1 to 3), a constant injection rate was maintained to minimize additional fracture propagation during circulation, as illustrated by the red curve in Figure 3. A large pressure buildup at the injection well, depicted by the blue curve, suggests significant formation resistance to fluid flow between the injector and the producer. The gray dots represent the measured production rates at the producer well 16B. Although the injection and production rates are plotted on separate axes, it is evident that the initial production rate was significantly lower than the injection rate, with a gradual increase observed over time. This pressure–rate behavior indicates that the initial three fracture stages in well 16A failed to generate sufficiently conductive pathways to the producer. Consequently, a large portion of the injected fluid was temporarily retained within the formation.

In the fiber-optic distributed strain rate waterfall plot, distinct tensile strain rate signals, indicated by red color, are observed within the zone of interest (Figure 4), reflecting an overall expansion of the formation in response to fluid injection. These strain responses were initially hypothesized to result from thermally induced stress, whereby the injection of cold fluid into the formation would lead to thermal contraction of the rock matrix and subsequent fracture opening. However, this mechanism does not fully explain the observed strain behavior. If thermal contraction were the dominant driver, one would also expect to observe compressive strain signatures associated with bulk rock shrinkage. Instead, the strain rate data predominantly exhibits tensile behavior, with no corresponding compressive regions evident in the plot. Furthermore, thermal induced deformation is insufficient to account for tensile strain signals

occurring only during specific intervals of the circulation test. These findings point to alternative mechanisms, such as pore pressure-driven mechanical responses or an increase in fracture width as the injection pressure is increased.

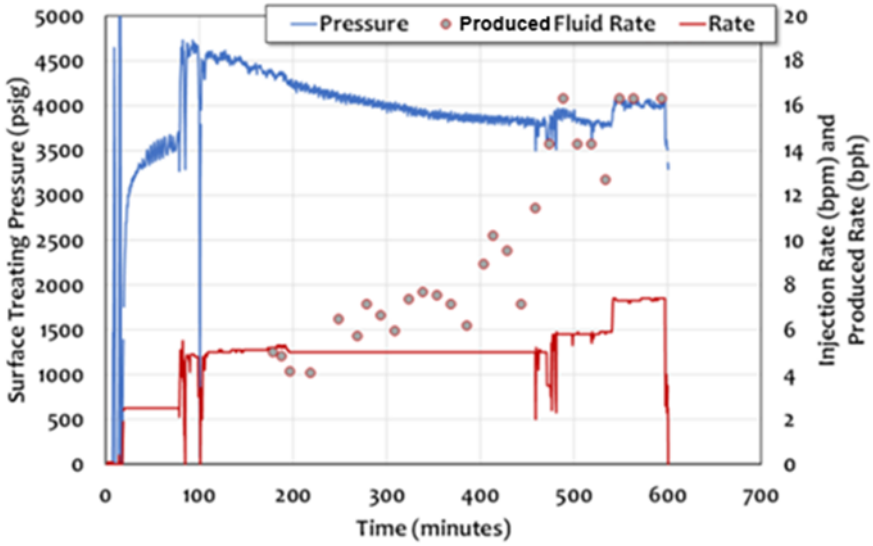


Figure 3: The rate-pressure data recorded during the second circulation test at the Utah FORGE site (Ou and Sharma, 2024)

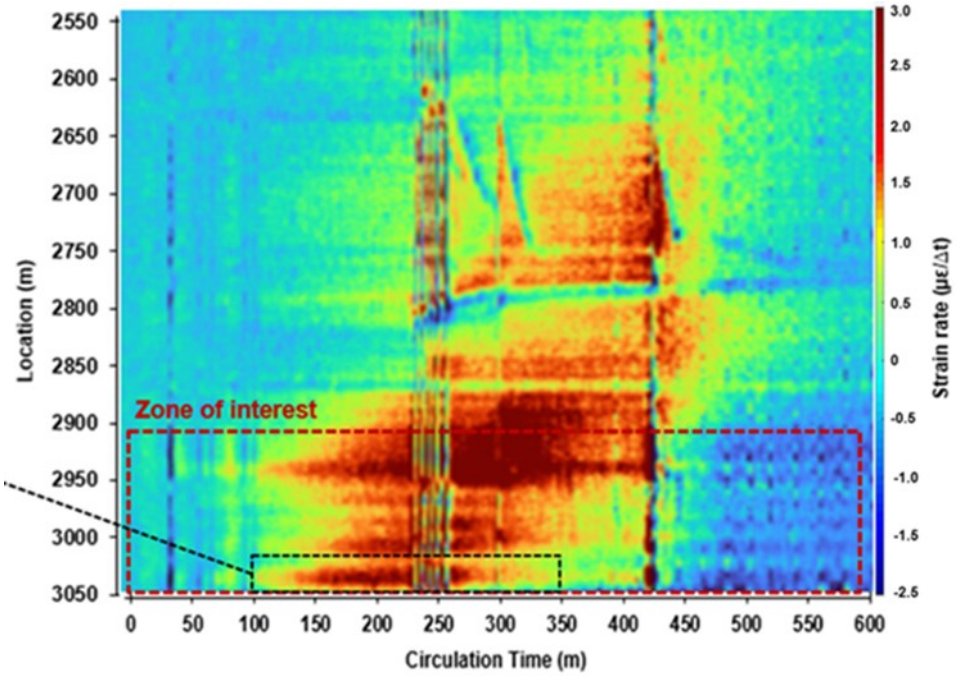


Figure 4: Approximate cross-well fracture intersections identified from fiber optic sensing data. Discrepancies between injector perforation locations and fracture intersections along the producer were identified, particularly in later stimulation stages (Modified from Jurick et al., 2025).

The initial fracture width (before fluid circulation) is small since the fracture supports the large difference in the minimum horizontal stress and fluid pressure within the fracture. This leads to low initial fracture conductivity and high formation resistance to fluid flow. A large pressure build-up is seen in the formation (Figure 3) as recorded in the field well injection data. As the pressure inside the fracture is increased by thousands of psi, the fracture will dilate during fluid circulation. Due to the gradual opening of the fracture and the fluid storage in the mechanical SRV, it takes hours (Figure 3) for the pressure build-up front to travel from the injector to the producer (formation compressibility is high within the surrounding SRV).

The fracture pressure, fracture width and fracture temperature distribution across the fracture surface at 3 selected simulation times are presented in Figure 5. The fracture pressure closely aligns with the fracture width evolution, as the fracture gradually opens along its

length as the pressure front travels through the fracture. Fracture conductivity increases with the opening of the fracture. The injection of cold fluid will decrease the temperature within the reservoir and fracture. Due to thermo-elasticity, the fracture width will also increase under the effect of reservoir cooling. Temperature change and thermal elasticity have a larger effect on fracture dilation but is mainly restricted near the injection well, while it also increases the injectivity of the fracture reservoir system. The fracture pressure and width evolution explain the production rate data that is recorded on the Forge site. The production rate generated from the circulation model Figure 6) has the same trend as the field production data. The overall production rate is small during the early stages of injection due to the small initial fracture width and fluid storage in the mechanical SRV. As is mentioned in Figure 6, the pressure front from the injector takes hours to reach the producer, and before that we do not see much fluid production. Production will gradually increase due to the gradual dilation of the fracture until the entire fracture-reservoir system stabilizes into a more conductive pathway for fluid to flow.

Pore pressure and the induced strain across the reservoir during EGS fluid circulation, are shown in Figure 8 during EGS fluid circulation. The strain rate is the signal that is monitored by the fiber optic cable at the producer. As the pressure front is travelling through the fracture, there is an induced tensional strain front travelling with the pressure front. There is also a second compressional strain front caused by the temperature change, but it takes a long time for it to be sensed by the fiber along the producer and is out of the scope of this work (cooling front will arrive much later after all the heat has been recovered from the rock). When the induced strain front reaches and passes by the producer (where the fiber is deployed), we clearly see the corresponding strain rate signal.

By plotting the strain rate along the production well against circulation time, the fiber optic strain rate waterfall plot is generated and depicted in Figure 9. The general drop-like shape of this modeling result matches well with the Forge fiber monitoring data for an anticipated single fracture region. This basically explains why the extensional strain rate signal occurs in the fiber monitoring plot within only a certain amount of time. It indicates the approaching and passing by of the tensional strain rate front at early transient fluid circulation.

Ou and Sharma (2024) modeled how the pressure and strain in the fracture evolve as the fluid is injected into the unpropped fracture. The simulation results were compared with the fiber optic strain rate signal can be used for evaluating the enhanced geothermal system in terms of fracture conductivity, the size of simulated reservoir volume and property changes within the SRV. These results showed that the pressure front travels faster in a well propped fracture with larger average conductivity, and the induced strain front arrives earlier at the fiber optic cable. When the fracture conductivity is higher, more injected fluid will directly flow through the fracture towards the producer instead of spreading into the surrounding SRV. The main factors control the changes in fracture conductivity over time are: proppant concentration, SRV compressibility, cluster spacing and rock Young's modulus.

The correspondence between strain rate responses and fracture properties confirms that the distributed strain data effectively identify the fractures that act as the primary flow pathways within the system. Although it remains challenging to identify "dead-end" fractures (fractures that intersect the production well but do not contribute to flow due to a lack of upstream connectivity) based solely on early-time fiber-optic responses, the distributed strain data provides valuable insight into the spatial variability in fracture conductivity across the stimulated zone. These results highlight the potential of distributed fiber-optic sensing to serve as a diagnostic tool for characterizing fracture conductivity and heterogeneity in multi-stage EGS developments.

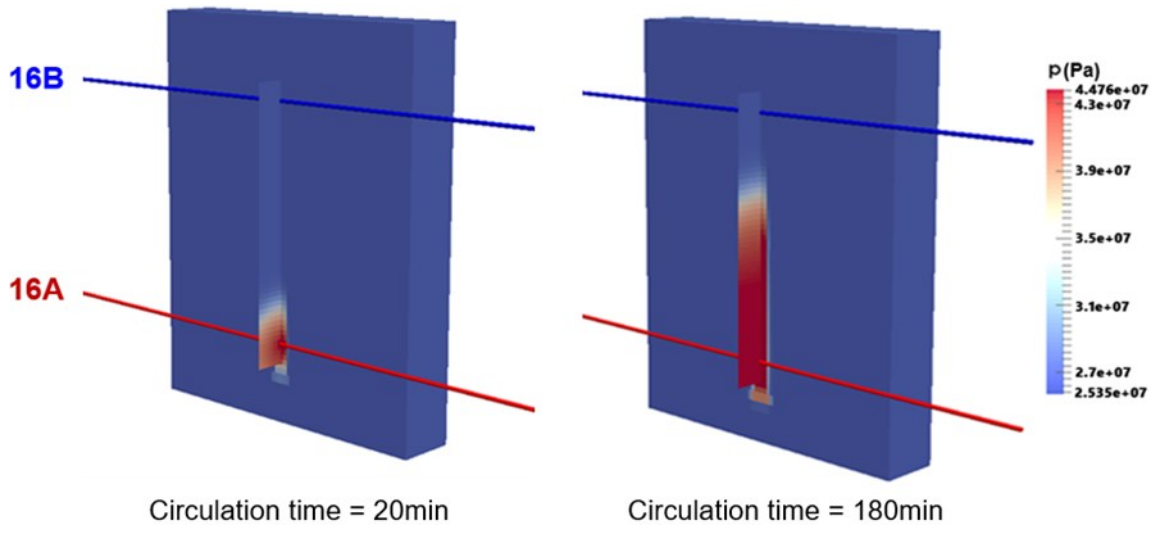


Figure 5: Formation pressure evolution during early fluid circulation for the Base Case. (a) A large pressure build up is seen at the fracture; (b) It takes hours for the pressure build up front to travel from the injector to the producer (Ou and Sharma, 2024).

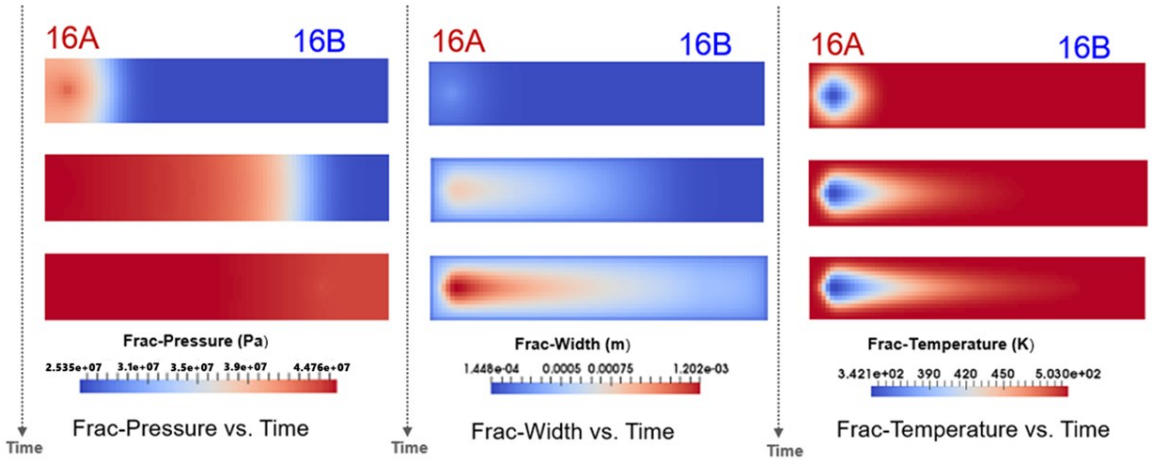


Figure 6: Fracture evolution during EGS circulation. (a) Fracture pressure evolution; (b) Fracture width evolution; (c) Fracture temperature evolution (Ou and Sharma, 2024).

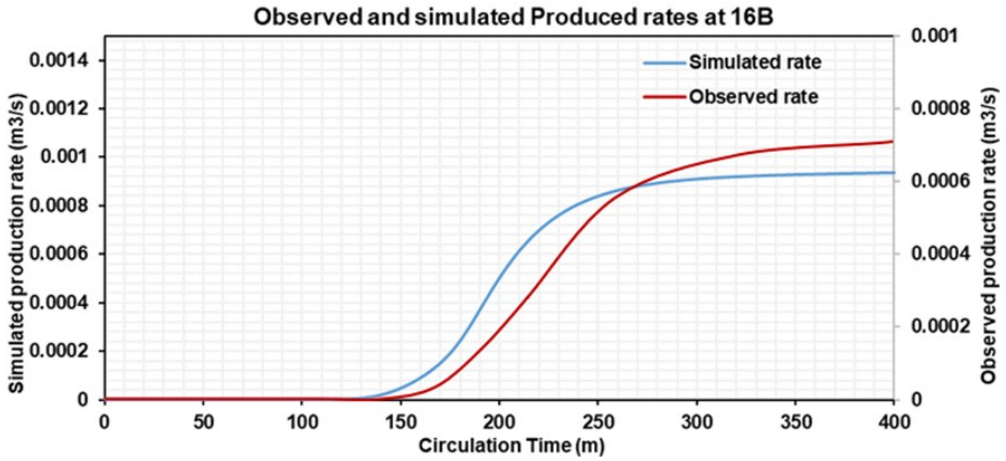


Figure 7: Averaged observed production rate and simulated production rate from the EGS producer (Ou and Sharma, 2024).

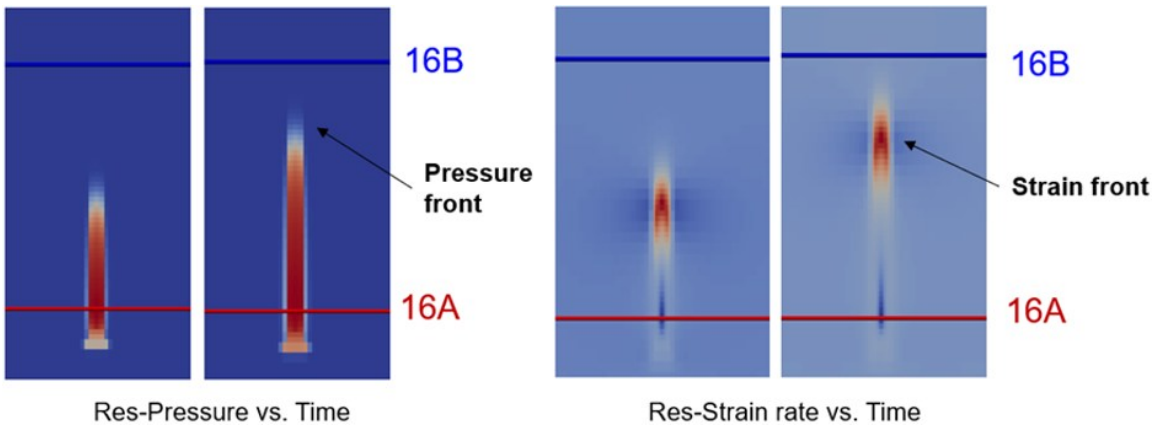


Figure 8: The induced strain front is traveling with the pressure front. (a) Pore pressure evolution; (b) The induced strain front evolution (Ou and Sharma, 2024).

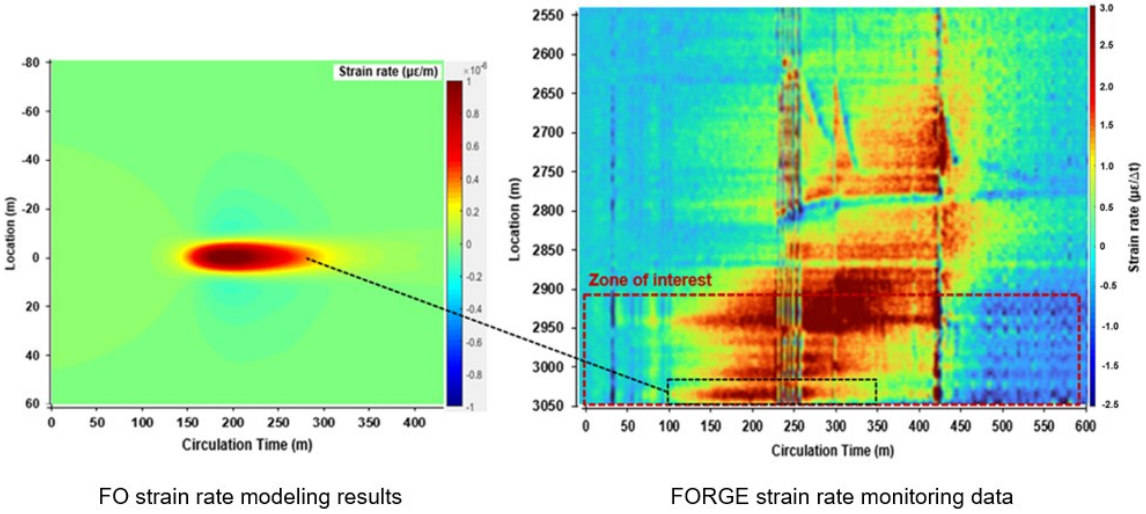


Figure 9: Modeling of fiber optic strain rate waterfall aligns well with field monitoring data during the circulation test. (a) Base Case fiber optic strain rate waterfall modeling results. (b) The field fiber optic monitoring data from the July 2023 circulation test (Ou and Sharma, 2024).

## 4. FRACTURE CONNECTIVITY

The connectivity of the fracture network to both the injector and the producer is essential for fluid circulation in EGS well pairs. It is often difficult to assess the degree of connectivity between wells. We used two independent methods to evaluate inter-well connectivity:

1. Thermal slugging signals in fiber optic data interpreted through numerical models.
2. Integration of fiber optic data with chemical tracer data for stage connections.

### 4.1 Thermal Slugging Velocity in the Fiber Optic Waterfall Data

The Rayleigh frequency shift based distributed strain sensing (DSS-RFS) and low-frequency DAS (LF-DAS) have demonstrated sensitivity to localized temperature perturbations, making them valuable tools for inflow profiling (Jin et al., 2019). Fiber-optic distributed sensing technologies can detect these perturbations via the propagation of transient thermal slugs along the wellbore during the early phases of production. When a shut-in well starts producing, the incoming fluid is at a different temperature to the previously stationary fluid, and the fiber experiences a measurable strain change. The subsequent displacement of this thermal contrast along the wellbore before reaching thermal equilibrium is referred to as thermal slugging (Mahue et al., 2022a).

Fiber-optic temperature measurements exhibit a linear correlation with borehole temperature, so the thermal slugging features observed in the diagnostic waterfall plot indicate the movement of fluid. Because these waterfall plots are presented as functions of depth and time, the velocity of the moving fluid can be inferred from the slope of the thermal slugs. By tracking multiple thermal slugs throughout the wellbore, it is possible to construct depth-dependent velocity profiles and evaluate near-wellbore inflow behavior (Mahue et al., 2022b).

Ou et al. (2025b) used a multi-domain numerical model, fully integrating the non-isothermal fluid within the entire reservoir-fracture-wellbore system, to simulate the April 2024 EGS fluid circulation test. The simulation results revealed that, prior to the April 2024 circulation test, both the fracturing treatment and in-well circulation introduced significant thermal heterogeneity along producer well 16B. Given the high sensitivity of fiber-optic sensing to localized temperature variations, the movement of fluids with varying thermal signatures during the early stages of circulation gave rise to a pronounced thermal slugging effect as shown in the fiber optic waterfall plot. The gradients of these thermal slugging signals in the fiber optic data were found to be reliable indicators of fluid velocities within different sections of the production well (Figure 10) and can be further processed to estimate the production rates from various fracture stages.

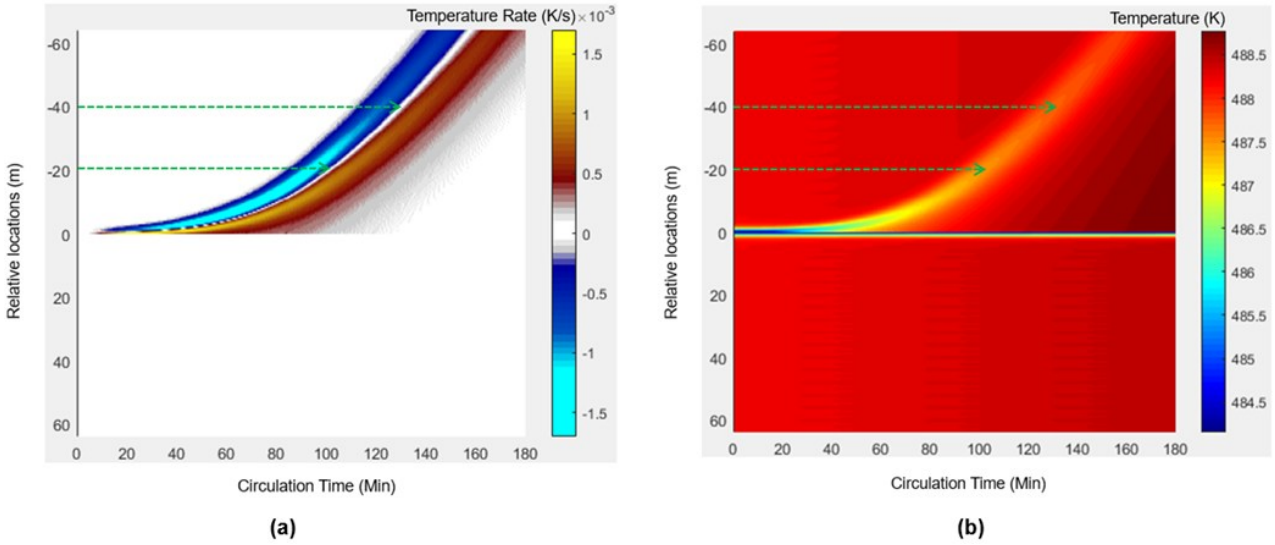


Figure 10: Thermal simulation waterfall plots of the single fracture case discussed by Ou et al. (2025b). (a) Simulated temperature change rate waterfall plot that represents the fiber optic monitoring data. (b) Production wellbore temperature waterfall plot during EGS circulation. The low-temperature fluid segment is moving towards the heel during early circulation.

### 4.2 Stage Connections Detected in Fiber Optic Data

Based on the fiber optic monitoring data acquired during the FORGE April 2024 well 16A stimulation as presented in Figure 11, the following conclusions can be drawn regarding the stage connections between injector 16A and producer 16B:

- Stage 1 in well 16B is apparently connected to Stage 3R, 4, 5 and 6 in well 16A.
- During the fracturing treatment of Stage 7 in well 16A, fracture reactivation signals were detected at the locations of previous fracture-driven interactions associated with Stage 6. Therefore, some fractures originating from Stage 7 in well 16A should overlap with fractures from Stage 6 and connect to Stage 1 in well 16B.
- Since Stage 7 in well 16A has 3 perforation clusters, this work assumes that one cluster within Stage 7 is redirected to previous fractures within Stage 6 and connected to the producer 16B at Stage 1. This assumption is consistent with the chemical tracer interpretation, which detected a flow connection between 16B Stage 1 and 16A Stage 7 as illustrated by the light blue line in **Fig. 13b**.
- During the fracturing treatment of Stage 8 in well 16A, fracture reactivation signals were detected at the locations of previous fracture-driven interactions associated with Stage 7. Given Stage 8 is perforated with 8 clusters, it is concluded that one cluster within Stage 8 is redirected to previous fractures within Stage 7 and connected to the producer 16B at Stage 2.
- The perfect match between one FDI signal during the stimulation of Stage 8 in well 16A and the thermal slugging signal of Stage 3 in well 16B suggests that another cluster of Stage 8 in well 16A is connected to Stage 3 in well 16B.
- During the fracturing treatment of Stage 9 in well 16A, fracture reactivation signals were detected at the locations of previous fracture-driven interactions associated with Stage 8. Given Stage 9 is also perforated with 8 clusters, it is proposed that two clusters within Stage 9 are redirected to previous fractures within Stage 8 and connected to the producer 16B at Stage 4.

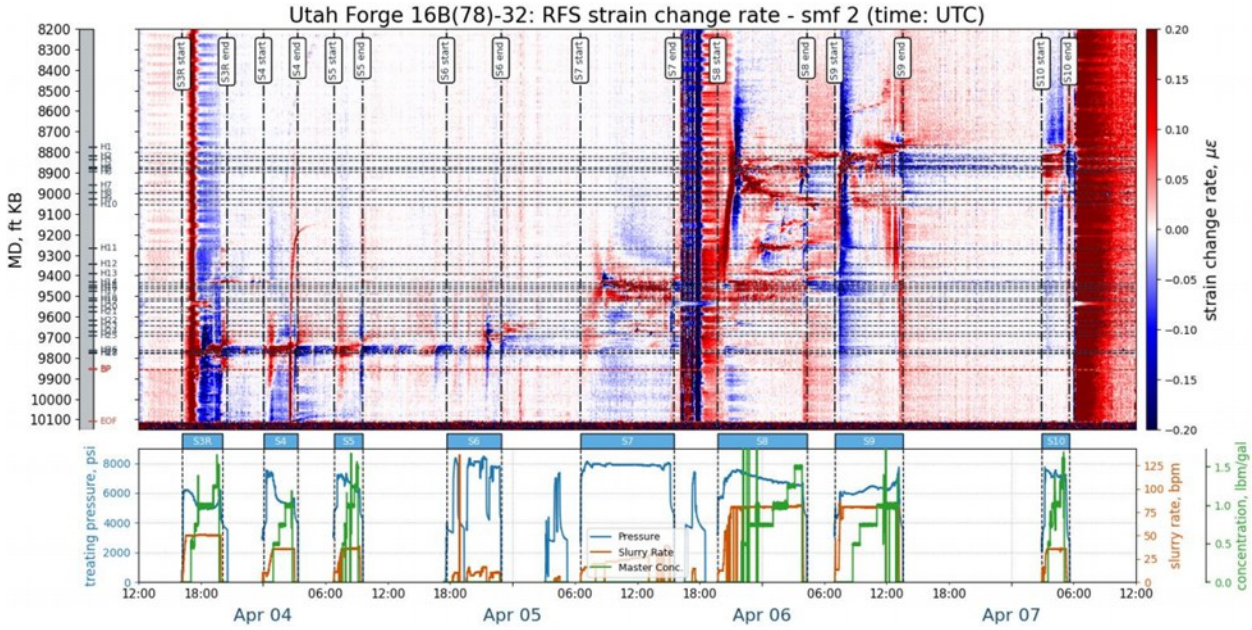


Figure 11: DSS-RFS strain change rate fiber optic monitoring along well 16B during the April 2024 stimulation of well 16A at the Utah FORGE site. (Jurick et al., 2025).

### 4.3 Stage Connections from Micro-seismic Data

Agreement between the pre-existing fractures observed in the FMI log and the fracture driven interactions detected in the fiber optic data suggest that fracture intersections at the producer 16B at the Utah FORGE site resulted from the reactivation of pre-existing fractures/faults. Nevertheless, the relatively sparse distribution of pre-existing fractures is not sufficient to explain another field observation that some clusters/stages are caught up by the same natural fractures and intersect the producer at identical locations. The overlapping of fracture propagation was also clearly reflected in the micro-seismic data (Figure 12) reported by Pankow et al (2025).

The micro-seismic clouds of Stage 3R, Stage 4, Stage 5 and Stage 6 coincide, while the micro-seismic clouds of the heel-side of Stage 8 overlaps that of Stage 9. Although the micro-seismic clouds of Stage 8 and 9 follow the same inclined fracture propagation plane, an obvious distance is seen between this fracture plane and the perforated clusters where the fractures initiate. The hypothesis of bedding plane redirection proposed by Srinivasan et al. (2025) can be adopted to address the overlapping fracture propagation where the fracturing fluid injection was redirected by large bedding planes to adjacent pre-existing fractures/faults. The recharged natural fractures were then reactivated and the corresponding fracture driven interaction signals were detected by the fiber optic cable along the producer 16B.

The stage connections between injector 16A and producer 16B are depicted in Figure 13a where the overlap of fractures in Stage 7 with Stage 6 and Stage 8 in well 16A agrees with the stage flow connections determined from the dynamic tracer response (Figure 13b). The flow connections measured from the dynamic tracer response provide confirmation of hydraulic connections between the various stages with each line representing at least one connection (i.e., the FDIs did not pinch off and lose conductivity after the stimulation treatments).

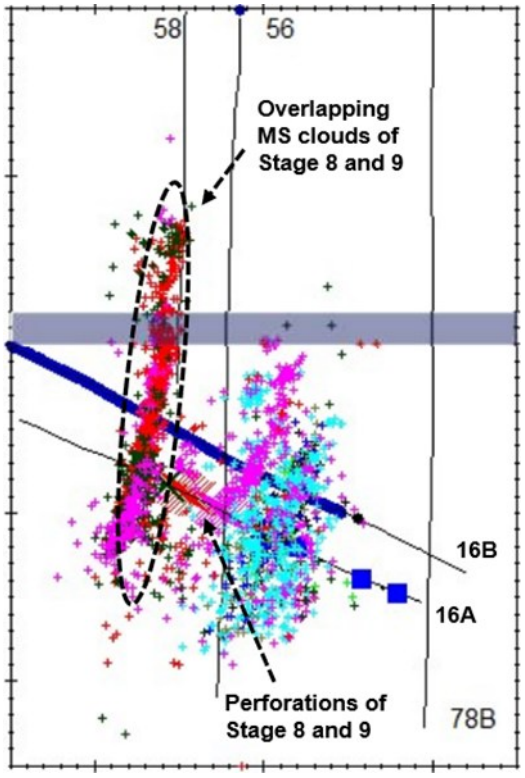


Figure 12: Micro-seismicity (MS) clouds data during the Utah FORGE April 2024 injection well stimulation (Pankow et al. 2025). The heel-side MS clouds of Stage 8 (depicted in pink color) follow the same inclined natural fracture with MS clouds of Stage 9 (depicted in red color).

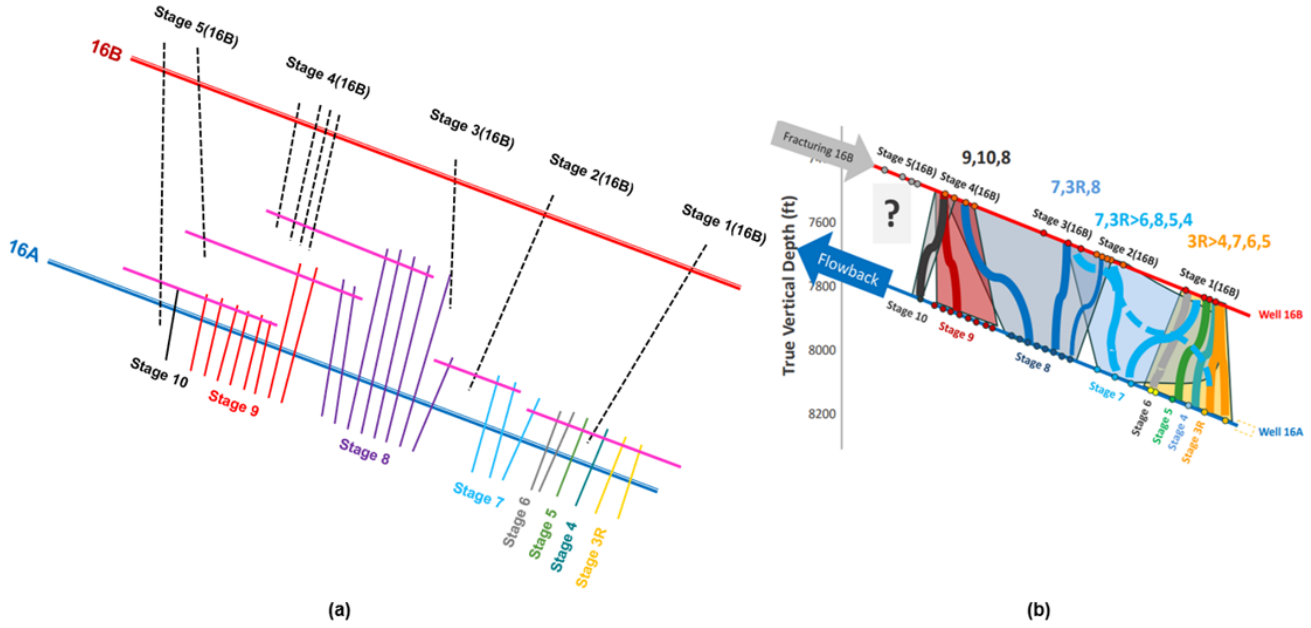


Figure 13: (a) Stage connections between injector 16A and producer 16B determined from the fiber optic data considering bedding plane (pink solid lines) and fracture-fault interaction. Black dashed lines represent pre-existing faults observed in the FMI log. (b) Stage flow connections determined from the dynamic tracer response (Fredd et al. 2025).

### 4.4 Stage Connections and Fiber Optic 16B Production Allocation

Production allocation for 16B well derived from the thermal slugging signals indicate that Stage 5, 4 and 1 exhibit higher production rates compared to Stages 2 and 3, particularly Stage 5 (Figure 14). This observation aligns with the completion design of the injector well 16A as shown on Figure 15. Stages 2 in well 16B intersects most of the fractures originating from Stages 7 of the injector well 16A, which was stimulated without the use of proppant. Stage 3 in well 16B is inferred to be hydraulically connected to a small number

of toe-side clusters from Stage 8 in well 16A. Fractures associated with Stage 3 are expected to exhibit poor conductivity. On the contrary, Stage 5 in well 16B intersects fractures from Stages 8, 9 and 10 of injector well 16A, all of which involved proppant injection into a larger number of perforated clusters (eight clusters were treated in Stage 8 and Stage 9). These contrasts in fracture conductivity and connectivity are clearly manifested in the thermal slugging signals associated with each production stage.

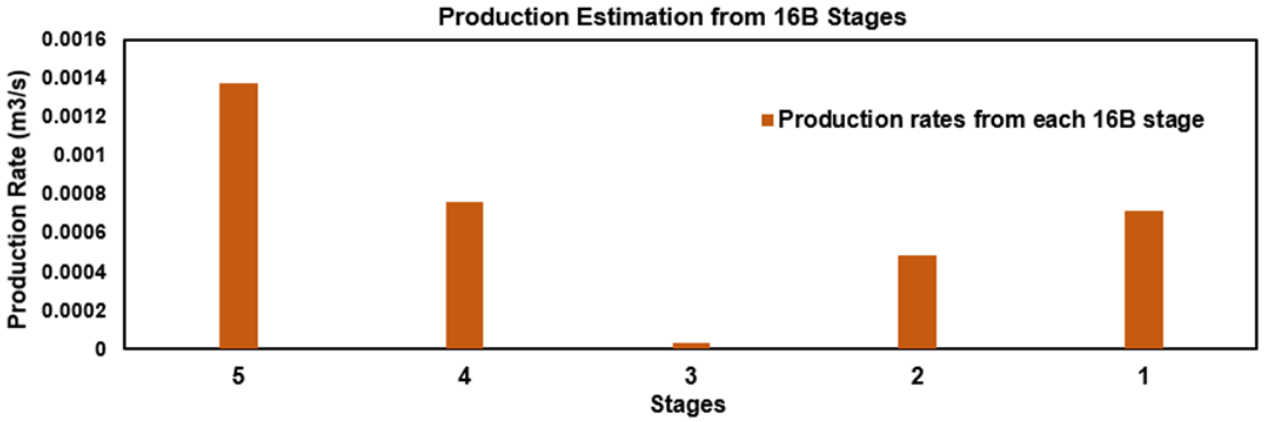


Figure 14: Production estimation along the production well 16B from fiber optic thermal slugging velocities (modified from Ou et al. 2025b).

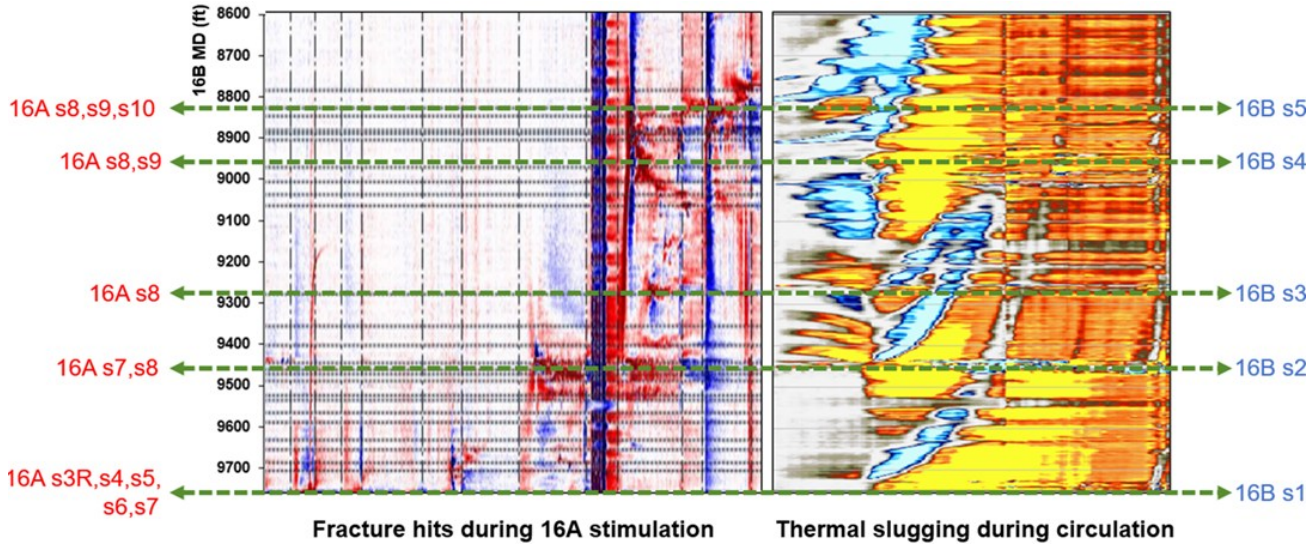


Figure 15: Comparison of fiber optic monitoring waterfall plots monitored during April 2024 16A stimulation and the following fluid circulation. The thermal slugging signals during early circulation originate from fracture intersection locations observed during the 16A stimulation. These main intersections are also locations where the production well is perforated.

## 5. FRACTURE CONFORMANCE

### 5.1 HF-DAS Data during the Stimulation of Well 16B

Figure 16 shows high frequency DAS data from Stage 3 in well 16B during its hydraulic fracturing treatments conducted in April 2024. This is a representative data set for one stage and results for other stages are shown in Appendix B. It is evident from the data that for all stages, the toe side clusters take proppant for only the early part of the treatment. After some time, the perforations screen out and no more fluid/proppant enters the toe side clusters, resulting in a very non-uniform placement of proppant in the treatment stage.

We simulated the fracture treatments in well 16B to explore how the treatments can be improved. As shown earlier. DAS data clearly indicate heel dominated fractures. Several completion and fracturing design parameters were changed to show that it is possible to get more uniform proppant placement in all the clusters.

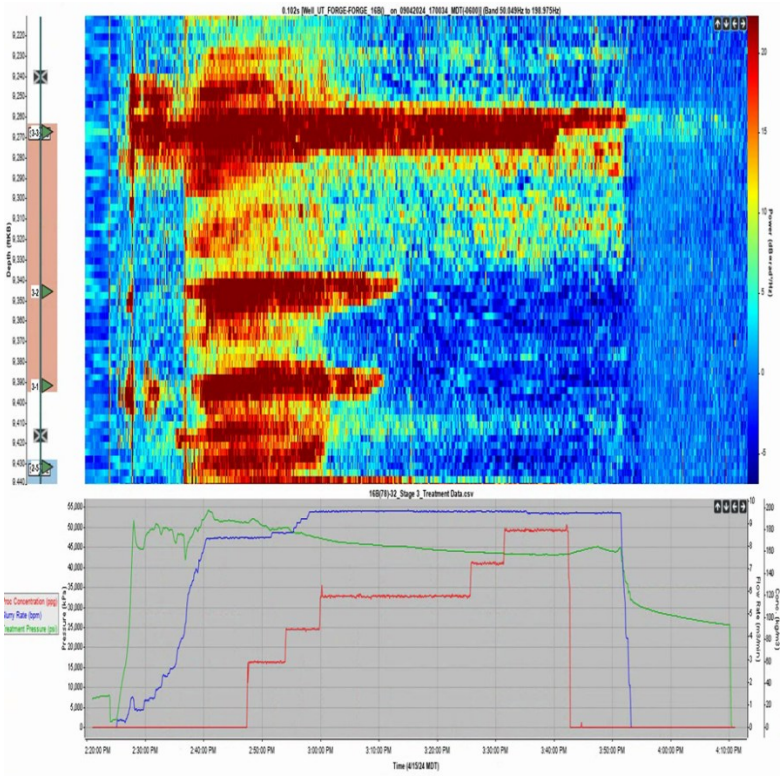

Figure 16: HF-DAS data during April 2024 stimulation of well 16B (Stage 3) at the Utah FORGE site. The fiber optic waterfall plot suggested a clear heel dominated fracture pattern where cluster screen-out happened at the locations of toe-side and middle cluster (Li et. al., 2026).

### 5.2 Modeling Well 16B

The Base Case represents the reference fracturing condition of Stage 3 in production well 16B stimulation. Figure 17a presents the final cluster-level fluid allocation. The results show that the heel cluster receives the largest fraction of injected fluid, while the toe cluster contributes the least, indicating strong non-uniformity along the stage. Figure 17b shows the final proppant allocation, which mirrors the fluid trend, most of the injected proppant accumulates near the heel cluster, while the toe cluster receives only a small fraction.

Figure 18 depicts the temporal evolution of fluid and proppant distribution among clusters. During the initial stages of pumping, the flow distribution is nearly uniform. However, as the injection continues and the local proppant concentration increases, bridging and deposition begin first near the toe perforations. The formation of local bridges restricts the effective flow area and causes a sharp decline in toe-side inflow. Once the toe cluster begins to plug, the injected fluid is diverted toward the middle and heel clusters. With time, the middle cluster also starts accumulating proppant, while the heel cluster remains the primary open flow path. This sequence matches the high-frequency DAS data (Figure 16), where toe-side acoustic energy decays earlier while heel-side strain signals persist for longer durations.

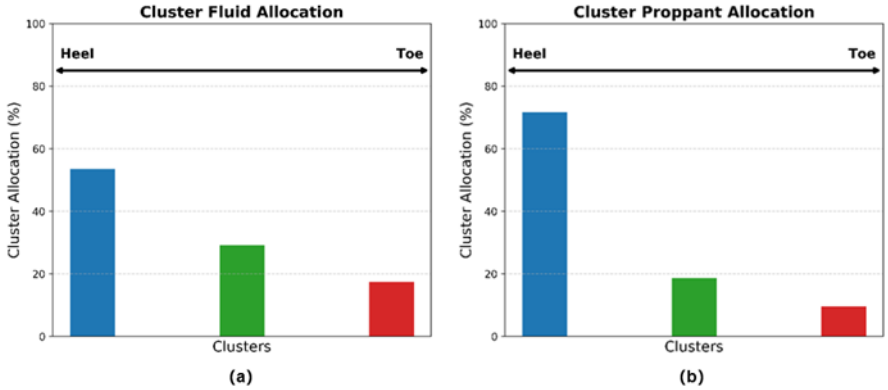


Figure 17: (a) Base Case final fluid allocation per cluster. (b) Base Case final proppant allocation per cluster (Li et. al., 2026).

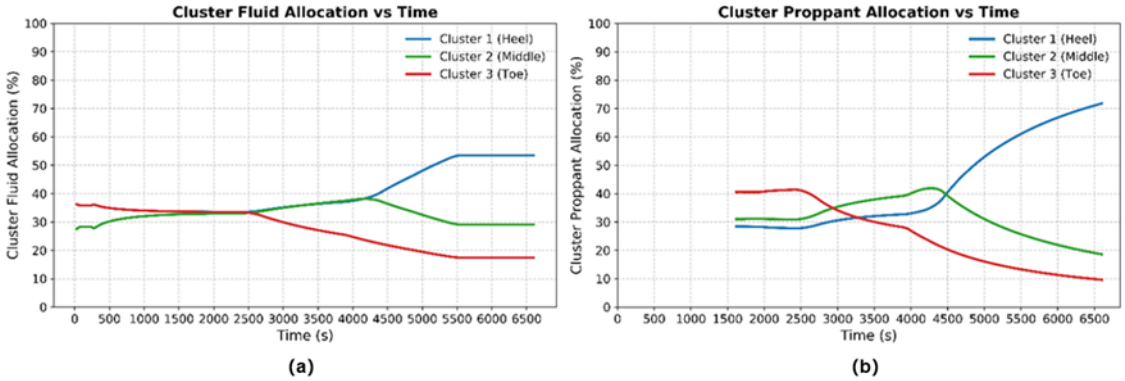


Figure 18: (a) Base Case fluid allocation vs time per cluster. (b) Base Case proppant allocation vs time per cluster (Li et. al., 2026)

### 5.3 Methods to Optimize Proppant and Fluid Distribution in Clusters

Achieving uniform fluid and proppant placement across perforation clusters is critical for maximizing fracture efficiency and ensuring balanced stimulation along the wellbore. By mitigating heel dominance and promoting even proppant transport, overall fracture conductivity and stage productivity can be significantly improved. In this study, three optimization strategies are proved to enhance near-wellbore flow distribution and improve proppant placement:

(1) The application of viscous carrier fluids to stabilize slurry transport and delay early bridging,

(2) The use of lightweight proppants to increase particle suspension time and reduce gravitational settling, and

(3) The adoption of a tapered perforation design to counteract wellbore pressure losses through hydraulic balancing.

## 6. CONCLUSIONS

The energy extraction rate in any EGS well pair is controlled by the three Cs:

- Conductivity of the created fracture network from the injector to the producer.
- Connectivity of the fracture network (between the injector and producer) through which the injected fluid flows.
- Conformance. Uniformly placed fractures to ensure an even distribution of flow into all hydraulic fractures.

We clearly show that by integrating fiber optic data with tracer and micro-seismic data it is possible to quantify these critical parameters. This comprehensive fracture diagnostics approach enabled us to monitor the performance of the injection-production well pair at Forge and conduct a detailed assessment of the effectiveness of different stimulation methods. This design methodology can result in better connected and more uniform fractures and have a transformational impact on geothermal energy extraction by increasing the rate of energy extraction and reducing the energy extraction decline rate.

## 8. REFERENCES

1. “Integration of Fiber Optic Data with FMI And Chemical Tracer Data to Evaluate Inter-well Fracture Connectivity and Fluid Circulation in Geothermal Well Pairs”, Y. Ou, Chris Fredd and Mukul Sharma, SPE Hydraulic Fracturing Conference, Feb. 2026.
2. “Strategies for Improving Inter-well Connectivity and Proppant Placement in EGS Well Pairs: A Field Study Integrating Models and Well Fiber Optic Data”, Y. Li, Y. Ou, M. Mura, Mukul Sharma, SPE Hydraulic Fracturing Conference, Feb. 2026.
3. “Pressure Drawdown Testing in Fractured Production Wells: Impact of Geomechanics and Fracture Closure”, Y. Li, Y. Ou, Mukul Sharma, SPE Hydraulic Fracturing Conference, Feb. 2026.
5. “Inversion Of Natural Fracture Properties Using Microseismic Data and Hydraulic Fracture Simulation”, Q. Liu and Mukul Sharma, SPE Hydraulic Fracturing Conference, Feb. 2026.
6. “Monitoring fluid circulation in an enhanced geothermal system with permanent fibers”, ARMA Workshop on Distributed Fiber Optic Sensing for Geomechanical Applications, Paper presented at the 58th US Rock Mechanics/Geomechanics Symposium held in Golden, Colorado, USA, 23-26, June 2024, Yuhao Ou and Mukul M. Sharma.
7. “Factors Controlling the Flow and Connectivity in Fracture Networks in Naturally Fractured Geothermal Formations,” SPE Drilling and Completions, Vol. 38, issue 01, pp 131-145, SPE-212292-PA, March 2023, M. Cao and M.M. Sharma. https://doi.org/10.2118/212292-PA.
8. “A computationally efficient model for fracture propagation and fluid flow in naturally fractured reservoirs,” Journal of Petroleum Science and Engineering, Vol. 220, Part B, pp 111249, January 2023, M. Cao and M.M. Sharma. https://doi.org/10.1016/j.petrol.2022.111249

9. “The impact of changes in natural fracture fluid pressure on the creation of fracture networks,” Journal of Petroleum Science and Engineering, Vol. 216, pp. 110783, September 2022, M. Cao and M.M. Sharma. https://doi.org/10.1016/j.petrol.2022.110783

10. “Creation of a Data-Calibrated Discrete Fracture Network of the Utah FORGE Site,” ARMA 23–0822, Paper was presented at the 57th US Rock Mechanics/Geomechanics Symposium held in Atlanta, Georgia, USA, 25-28 June 2023, M. Cao and M.M. Sharma.

11. “Integrating a Boundary Element Method Based Hydraulic Fracturing Simulator with a Compositional Reservoir Simulator for Well Lifecycle Simulations,” ARMA 23–0382, Paper was presented at the 57th US Rock Mechanics/Geomechanics Symposium held in Atlanta, Georgia, USA, 25-28 June 2023, M. Cao, S. Zheng, and M.M. Sharma.

12. “Geomechanical Modeling of Fracture Growth in Naturally Fractured Rocks: A Case Study of the Utah FORGE Geothermal Site,” Paper presented at the Unconventional Resources Technology Conference held in Denver, Colorado, USA, 13-15 June 2023, M. Cao and M.M. Sharma.

13. “The Effect of Variations of Fluid Pressure in Natural Fractures on the Geometry of Fracture Networks and Well Productivity,” Paper presented at the Unconventional Resources Technology Conference held in Denver, Colorado, USA, 13-15 June 2023, M. Cao and M.M. Sharma.

14. “Factors Controlling the Flow and Connectivity in Fracture Networks in Naturally Fractured Geothermal Formations,” SPE Drilling and Completions, Vol. 38, issue 01, pp 131-145, SPE-212292-PA, March 2023, M. Cao and M.M. Sharma. https://doi.org/10.2118/212292-PA

15. “A computationally efficient model for fracture propagation and fluid flow in naturally fractured reservoirs,” Journal of Petroleum Science and Engineering, Vol. 220, Part B, pp 111249, January 2023, M. Cao and M.M. Sharma. https://doi.org/10.1016/j.petrol.2022.111249

16. “An Efficient Model of Simulating Fracture Propagation and Energy Recovery from Naturally Fractured Reservoirs: Effect of Fracture Geometry, Topology and Connectivity,” SPE-212315-MS, Paper presented at the SPE Hydraulic Fracturing Technology Conference and Exhibition, January 31–February 2, 2023, M. Cao and M.M. Sharma, doi: https://doi.org/10.2118/212315-MS

17. “The impact of changes in natural fracture fluid pressure on the creation of fracture networks,” Journal of Petroleum Science and Engineering, Vol. 216, pp. 110783, September 2022, M. Cao and M.M. Sharma. https://doi.org/10.1016/j.petrol.2022.110783

18. Mahue, V., Jimenez, E., Dawson, P., Trujillo, K., and Robert, H. 2022a. Repeat DAS and DTS Production Logs on a Permanent Fiber Optic Cable for Evaluating Production Changes and Interference with Offset Wells. Paper presented at the SPE/AAPG/SEG Unconventional Resources Technology Conference, Houston, Texas, USA, June. https://doi.org/10.15530/urtec-2022-3725993

19. Mahue, V., Dawson, P., Jimenez, E., Kiyoumi, A., Tamimi, A., Othman, A., Correia, G., Alyan, M., and Shardul, P. 2022b. Advances in an Integrated Analysis Workflow of Distributed Acoustic Sensing and Distributed Temperature Sensing for Water Injection Profiling on a Horizontal Well. In ADIPEC, Abu Dhabi, UAE, October. https://doi.org/10.2118/211584-MS